Journal of Non-Crystalline Solids 496 (2018) 6–12

Contents lists available at ScienceDirect

Journal of Non-Crystalline Solids

journal homepage: www.elsevier.com/locate/jnoncrysol

# The effect of alkali metal ions on crystallization characteristics and luminescent properties of transparent $Er^{3+}$-doped fluorosilicate glass-ceramics

Qinpeng Chen[a,b], Xiaoqian Song[a,b], Shiliang Kang[a,b], Jianrong Qiu[c], Guoping Dong[a,b,*]

[a] State Key Laboratory of Luminescent Materials and Devices, and Guangdong Provincial Key Laboratory of Fiber Laser Materials and Applied Techniques, South China University of Technology, Guangzhou 510640, China
[b] Guangdong Engineering Technology Research and Development Center of Special Optical Fiber Materials and Devices, School of Materials Science and Engineering, South China University of Technology, Guangzhou 510640, China
[c] College of Optical Science and Engineering, State Key Laboratory of Modern Optical Instrumentation, Zhejiang University, Hangzhou 310027, China

ARTICLE INFO

*Keywords:*
Alkali metal ions
Glass-ceramics
$Er^{3+}$
Mid-infrared luminescence

ABSTRACT

In current work, transparent fluorosilicate glass-ceramics (GCs) containing $NaYF_4$:$Er^{3+}$ nanocrystals were successfully prepared by controlled heat treatment process. The thermal properties and crystallization characteristic temperatures were determined by the differential scanning calorimetry (DSC). The X-ray diffraction (XRD) and transmission electron microscope (TEM) were used to confirm the formation of $NaYF_4$ nanocrystals in glass matrix. Energy dispersive spectrometer (EDS) results and Judd-Ofelt (J-O) parameters analysis demonstrated the incorporation of $Er^{3+}$ into $NaYF_4$ nanocrystals. Intense 2.7 μm luminescence was observed in $Er^{3+}$-doped GCs upon excitation with a 980 nm laser diode (LD). Furthermore, the effect of different alkali metals ($Li^+$, $Na^+$, $K^+$) on crystallization characteristics and luminescent properties has been studied in detail, which indicates $Li^+$ is the most favorable option for mid-infrared luminescence properties compared with $Na^+$ and $K^+$. The excellent spectroscopic characteristics suggest that the obtained GCs may be promising materials for mid-infrared fiber lasers.

## 1. Introduction

The range of mid-infrared (MIR) band is from 2 to 5 μm, which located in the region of thermal infrared remote sensing. The potential applications of MIR fluorescence highly attach researchers' attention [1–3]. The transmittance in the range of MIR band is high in atmosphere, which can be used in the area of remote sensing, defense, satellite and other optical fields [4–7]. Because of a strong absorption peak in the MIR band of many molecules, the MIR fluorescence also have promising prospects in the air pollution detection, detection of pollutants and other medical fields [8–10].

Due to rich energy level structure, $Er^{3+}$ can be excited by not only ultraviolet light and visible light, but also 808 nm and 980 nm commercial lasers [11]. Under the excitation of pumping light source, 2.7 μm MIR fluorescence can be obtained by the $^4I_{11/2} \rightarrow {}^4I_{13/2}$ transition of the $Er^{3+}$ ions. The 2.7 μm MIR fluorescence emission of $Er^{3+}$ depends on the intensity of the $^4I_{11/2} \rightarrow {}^4I_{13/2}$ radiation transition as well as the distribution of the electron in the upper and lower energy levels [12]. The interval of $Er^{3+}$:2.7 μm MIR emission energy level is narrow, which is sensitive to the phonon energy of the matrix material. High phonon energy of the matrix material increases the phonon relaxation rate, resulting in the self-quenching of radiation transition and decrease of the luminous intensity of $Er^{3+}$:2.7 μm MIR emission [13]. Therefore, in order to fabricate the efficient $Er^{3+}$ MIR fluorescent laser materials, it is necessary to search the matrix materials with high luminous efficiency, good chemical stability and good mechanical properties [14–18].

In a large number of matrix materials, the glass-ceramic (GC), combining the workability of glass and the low phonon energy of crystal field, is expected to obtain the high-efficiency GC fiber in MIR fluorescence band [20–23]. Moreover, GC also plays a role in some cutting-edge fields, such as the dentistry and laser cooling, etc. [18,19]. As we know, the alkali metal oxide, a typical network modifiers, deeply affect the glass forming performance and crystallization performance of the glass. But at present, there is few systematic study of the effect of different alkali metal ions on crystallization characteristics and

* Corresponding author at: State Key Laboratory of Luminescent Materials and Devices, and Guangdong Provincial Key Laboratory of Fiber Laser Materials and Applied Techniques, South China University of Technology, Guangzhou 510640, China.
*E-mail address:* dgp@scut.edu.cn (G. Dong).

https://doi.org/10.1016/j.jnoncrysol.2018.05.010
Received 29 March 2018; Received in revised form 4 May 2018; Accepted 5 May 2018

**Table 1**
Specific thermal treatment temperatures of SL, SN and SK.

| Samples | $T_g$ (°C) | $T_x$ (°C) | ΔT (°C) | Heat treatment temperature (°C) |
|---|---|---|---|---|
| $39SiO_2$-$25Al_2O_3$-$18Na_2O$-7LiF-$10YF_3$-$1ErF_3$ (SL) | 514 | 644 | 130 | 600, 610, 620, 630 |
| $39SiO_2$-$25Al_2O_3$-$18Na_2O$-7NaF-$10YF_3$-$1ErF_3$ (SN) | 517 | 671 | 154 | 630, 640, 650, 660 |
| $39SiO_2$-$25Al_2O_3$-$18Na_2O$-7KF-$10YF_3$-$1ErF_3$ (SK) | 552 | 712 | 160 | 650, 660, 670, 680 |

luminescent properties of glass-ceramics. So, it is necessary for us to study in this aspect mentioned above.

In this paper, transparent fluorosilicate glass-ceramics containing $NaYF_4$:$Er^{3+}$ nanocrystals as well as different alkali metal ions ($Li^+$, $Na^+$ and $K^+$) have been prepared. The effects of alkali metal ions ($Li^+$, $Na^+$ and $K^+$) on the crystallization characteristics and 2.7 μm MIR luminescent properties were studied in detail.

## 2. Experimental

The precursor glasses with the molar composition of $39SiO_2$-$25Al_2O_3$-$18Na_2O$-7MF-$10YF_3$-$1ErF_3$ (M = Li, K and Na) were fabricated by the conventional melt-quenching technique. The samples were named as Sample-Li(SL), Sample-Na(SN) and Sample-K(SK), respectively. For each batch, about 30 g of original materials was fully mixed and melted in a covered alumina crucible in air atmosphere at 1500 °C for 1 h. The melt was then poured onto a preheated copper plate and pressed into a glass sheet. After annealing at 450 °C for 2 h to release inner stress, the glass samples were heat-treated at different temperatures for 4 h to obtain GCs. The specific thermal treatment temperature is determined by the data of DSC, as shown in the following Table 1. All samples, including the precursor glasses and the GCs, were cut and polished for performance characterization, and the size of the glass plate is about 10 mm × 10 mm × 1.5 mm.

In order to determine the crystallization characteristic temperatures, the differential scanning calorimetry (DSC) was carried out in a comprehensive thermal analyzer (STA449C NETZSCH) under $N^2$ atmosphere with the 10 °C/min heating rate. X-ray Diffraction (XRD) analysis was performed on an X'Pert PRO X-ray diffractometer by using Cu Kα$_1$ as a radiation source to identify the crystalline phase and estimate the nanocrystal grain size. Transmission electron microscope (TEM, 2100F, JEOL, Japan) equipped with energy-dispersive spectrometer (EDS) system was conducted to analyze the microstructure and the elements distribution of GC samples. The absorption spectra were measured in the range of 500–3200 nm using a Perkin-Elmer Lambda 900/UV/VIS/NIR spectrophotometer. The mid-infrared (MIR) luminescence spectra pumped by 980 nm laser diode (LD) in the range of 2500–2900 nm were measured on a spectrometer (zolix, Omni 5015i, Beijing, China) with a lock-in amplifier. The fluorescence decay curves of $Er^{3+}$: $^4I_{11/2}$ and $^4I_{13/2}$ levels were captured by a Tektronix TDS 3012c Digital Phosphor Oscilloscope with pulsed 808 and 980 nm LDs as excitation sources, respectively. All the measurements were carried out at room temperature.

## 3. Results and discussion

The DSC curves of the SL, SN and SK are presented in Fig. 1. The glass transition temperature ($T_g$) of SK (552 °C) is the highest, followed by that of SN (517 °C), and that of SL (514 °C) is the lowest. The crystallization temperature ($T_x$) also has the same rule. According to the DSC curves, the heat treatment schedule of the SL, SN and SK were designed, as shown in the Table 1. When alkali metal ions are added to the matrix glass, the alkali metal ions are bonded to the $O^{2-}$ ions in the

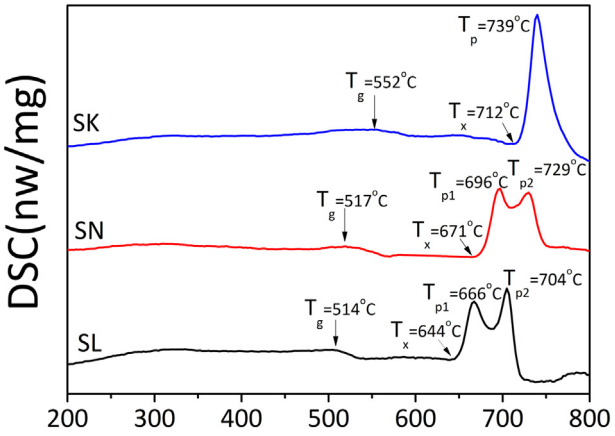


**Fig. 1.** DSC curves of SL, SN and SK.

glass network to form polar groups. With the oxidability of the $Li^+$, $Na^+$ and $K^+$ increasing in sequence, the bond between alkali metal with oxygen becomes stronger, which cause the increase of the $T_g$ and $T_x$. In addition, the ΔT is defined as the temperature gradient between $T_g$ and $T_x$, commonly used as a criteria to estimate thermal stability of glass qualitatively. From the DSC curves, it can be found that the glass become more thermally steadily as the atomic number of alkali metal increases.

Fig. 2 show the XRD patterns of precursor glasses and the GCs of the different samples. The precursor glasses are completely amorphous with no obvious diffraction peaks. In contrast, after a thermal treatment process at lower temperature, obvious sharp diffraction peaks are observed, which are assigned to the cubic α-$NaYF_4$ phase (JCPDS: 06-0342). With the increase of thermal treatment temperature, the diffraction peaks become more evident and sharper, indicating the gradual growth of $NaYF_4$ nanocrystals. However, with the further increase of thermal treatment temperature, other crystalline phases $SiO_2$ and hexagonal β-$NaYF_4$ appear.

The average crystallite size was estimated from the full width at half maximum (FWHM) of X-ray diffraction lines by using the Scherrer's equation [24]:

$$D_{hkl} = \frac{K\lambda}{\beta \cos\theta} \quad (1)$$

where $K$ is a constant of 0.89, λ represents the wavelength of Cu K$\alpha$ radiation whose value is 0.154056 nm, $\theta$ is the Bragg angle and $\beta$ is the FWHM intensity of the diffraction peak.

The diffraction peak used for the formula calculation is located at the 28.4°, which is assigned to the (111) plane of the cubic α-$NaYF_4$ nanocrystal. And the calculated average crystallite sizes are shown in the Table 2. The crystal size of precipitated nanocrystals in SL is also significantly larger than that of SN and SK. The different crystallization performance was produced by the different ionic radii and the ions potential (Z/r). In the glass network structure, if the field strength of the network modifiers is powerful enough, the modifiers will attract part of anions to form the enrichment area of certain compounds. Furthermore, it will cause the liquid-liquid phase separation in the glass melt macroscopically. As for the alkali metal ions, due to the smallest ion radii and the most powerful field strength, the incorporation of $Li^+$ promote the appearance of phase separation in the glass melt. And when the precursor glass of SL was heat treated to obtain the glass-ceramic, the existence of the phase interface would provide a platform for the crystal nucleation, which reduced the critical nucleation energy and critical nucleation radii [25]. Therefore, the incorporation of $Li^+$ contributes to the crystallization of the cubic α-$NaYF_4$ phase.

Fig. 3(a) shows the TEM image of SN heat-treated at 630 °C for 4 h. It can be observed that the dark particles are homogeneously dispersed